

To appear in *The Astrophysical Journal*

Coexistence of Gravitationally Bound and Radiation Driven C IV Emission Line Regions in Active Galactic Nuclei

Huiyuan Wang^{1,2}, Tinggui Wang^{1,2}, Hongyan Zhou^{1,2,6}, Bo Liu^{1,2}, Jianguo Wang³, Weimin Yuan⁴ and Xiaobo Dong^{1,2,5}

ABSTRACT

There are mutually contradictory views in the literature of the kinematics and structure of high-ionization line (e.g. C IV) emitting regions in active galactic nuclei (AGNs). Two kinds of broad emission line region (BELR) models have been proposed, outflow and gravitationally bound BELR, which are supported respectively by blueshift of the C IV line and reverberation mapping observations. To reconcile these two apparently different models, we present a detailed comparison study between the C IV and Mg II lines using a sample of AGNs selected from the Sloan Digital Sky Survey. We find that the kinematics of the C IV region is different from that of Mg II, which is thought to be controlled by gravity. A strong correlation is found between the blueshift and asymmetry of the C IV profile and the Eddington ratio. This provides strong observational support for the postulation that the outflow is driven by radiation pressure. In particular, we find robust evidence that the C IV line region is largely dominated by outflow at high Eddington ratios, while it is primarily gravitationally bounded at low Eddington ratios. Our results indicate that these two emitting regions coexist in most of AGNs. The emission strength from these two gases varies smoothly

¹Key Laboratory for Research in Galaxies and Cosmology, University of Science and Technology of China, Chinese Academy of Sciences, Hefei, Anhui 230026, China; whywang@mail.ustc.edu.cn

²Department of Astronomy, University of Science and Technology of China, Hefei, Anhui 230026, China

³National Astronomical Observatories/Yunnan Observatory, Chinese Academy of Sciences, P.O. Box 110, Kunming, Yunnan 650011, China

⁴National Astronomical Observatories, Chinese Academy of Sciences, Beijing 100012, China

⁵The Observatories of the Carnegie Institution for Science, 813 Santa Barbara Street, Pasadena, CA 91101, USA

⁶Polar Research Institute of China, Jinqiao Rd. 451, Shanghai, 200136, China

with Eddington ratio in opposite ways. This explanation naturally reconciles the apparently contradictory views proposed in previous studies. Finally, candidate models are discussed which can account for both, the enhancement of outflow emission and suppression of normal BEL, in AGN with high Eddington ratios.

Subject headings: line:profile – line:formation– quasars: emission lines – quasars: general

1. Introduction

It is now generally believed that super-massive black holes reside in the center of active galactic nuclei (AGNs; Lynden-Bell 1969). Through accretion of gas, AGNs release vast radiant energy, including high-energy ionizing photons, from an accretion disk around the black hole (Rees et al. 1984). The radiation photoionizes and heats surrounding gas so that it is able to leave its imprint, for example broad emission line (BEL) and broad absorption line (BAL), on the emergent continuum spectra emitted by accretion disk (Davidson & Netzer 1979; Osterbrock 1989; Weymann et al. 1991). The observed properties of these lines, such as strength, width, and profile, are determined by the combined effects of various physical processes. Hence, studies of these line features can reveal the physical conditions and processes in the central region of AGNs, and further shed light on the accretion and radiation mechanisms, and the co-evolution of black holes and their host galaxies.

The broad emission line region (BELR) is the most studied structure of AGNs. Extensive efforts had been devoted to probing its structure and kinematics, which are important for estimation of black hole masses and understanding of line formation. Velocity-resolved reverberation mapping of several local AGNs shows that there is no significant difference in the temporal response of the blue and red parts of the BELs to variations in the continuum (Gaskell 1988; Koratkar & Gaskell 1991; Korista et al. 1995; Done & Krolik, 1996; O’Brien et al. 1998). These studies demonstrate that the predominant motion of the BELR is either Keplerian or virial motion, both driven by the gravity of the central black hole (see Gaskell 2009, for a review). Further robust evidence supporting this view is given by the correlation between the BELR size and line width in the form $r \propto \sigma^{-2}$ for various emission lines found in a few well-studied AGNs (Krolik et al 1991; Peterson & Wandel 1999; 2000; Onken & Peterson 2002). This correlation is readily expected for gravitation dominated kinematics. Particularly, these works showed that the emitting regions of both high- and low-ionization lines (e.g. C IV and H β) are gravitationally bound.

However, studies of luminous AGNs at high redshifts uncover quite different behaviors

of the BELR, especially the high-ionization line (e.g. C IV) region. Gaskell (1982; see also Wilkes 1984; Marziani et al. 1996) found that the peak of the C IV line tends to be blueshifted with respect to the peak of low-ionization lines in a small sample of high-redshift AGNs. This was confirmed by Richards et al. (2002; also Vanden Berk et al. 2001) using a large sample of AGNs selected from the Sloan Digital Sky Survey (SDSS; York et al. 2000). Subsequently, the C IV blueshift was detected in several low-luminosity AGNs (e.g. Leighly & Moore 2004). The blueshift is difficult to reconcile with gravitationally bound BELR models, but is considered as a signature of outflowing gas (Gaskell 1982; Marziani et al. 1996; Leighly 2004). Outflow models based on dynamical and photoionization calculations have been put forward to reproduce the observed line profiles, equivalent widths and line ratios, and further imposing constraints on the density, ionization state and geometry of the line emitting gas (e.g. Murray & Chiang 1997; Leighly 2004; Wang et al. 2009b). In fact, the frequent occurrences of blueshifted narrow absorption lines and BALs in AGN spectra have proved that outflow is ubiquitous in AGN (Weymann et al. 1991; Crenshaw, Kraemer & George 2003). Outflow is therefore a natural interpretation of blueshift of high-ionization lines.

Although there have been a few attempts to tune one single model, i.e. outflow or gravitationally bound BELR, to simultaneously account for the contradictory observational results in reverberation-mapped objects and blueshifted C IV AGNs (e.g. Chiang & Murray 1996; Gaskell & Goosmann 2008), the dramatic inconsistency may indeed manifest fundamental differences in the structure and kinematics of these two line emitting regions. If this is the case, it would be interesting to find out what causes such differences. Previous studies have already provided some meaningful observational constraints on the underlying processes. For example, it is well known that the blueshift of the C IV emission line in radio quiet AGNs is, on average, stronger than in radio loud AGNs (Marziani et al. 1996; Sulentic et al. 2000a; Richards et al. 2002; 2011). Recently, several studies found that the C IV blueshift decreases with the increase of the X-ray to UV flux ratio (Gibson, Brandt & Schneider 2008; Richards et al. 2011). In addition, Sulentic et al. (2007) found that the correlation between the width and equivalent width of the C IV BEL varies dramatically with the width of the $H\beta$ BEL. Richards et al. (2011) found that C IV blueshift varies with the ionizing spectral energy distribution. All these facts point towards that BELR structure is related to the accretion process of the central engine.

It is worthwhile to note that the low-ionization lines, such as Mg II and $H\beta$, are fairly close to the systemic redshift (Marziani et al. 1996; Sulentic et al. 2000a; Richards et al. 2002). Apparently different from the high-ionization lines, the low-ionization line region is gravitationally bound, and outflow model is unlikely. This is supported by the fact that local AGNs follow the same luminosity-BELR size relationship for the $H\beta$ line as for those

well-studied AGNs, whose BELR have been demonstrated to be governed by gravity (Kaspi et al. 2005; Bentz et al. 2006). In particular, the power-law slope of this relationship is about 0.5, indicating that all of these AGNs have roughly the same ionization state and gas density in the low-ionization lines region. The $H\beta$ and $Mg\ II$ lines are therefore widely adopted to estimate the black hole masses, M_{BH} , of AGNs (Kaspi et al. 2000; Collin et al. 2006; Vestergaard & Peterson 2006; McLure & Jarvis 2002; Onken & Kollmeier 2008; Wang et al. 2009a). The M_{BH} estimate is plagued by many uncertainties in, for example, the geometry, kinematics and inclination of the BELR, the measurement of line width, the influence from other forces (such as radiation pressure), the validity of extrapolating the small-sample results to a large sample (Krolik 2001; Collin et al. 2006; Marconi et al. 2008; Richards et al. 2011). Although the M_{BH} estimate can be calibrated using the correlation between M_{BH} and bulge/spheroid stellar velocity dispersion (e.g. Onken et al. 2004), it is accurate only from a statistical point of view.

In this paper, we probe the structure and kinematics of the high-ionization line emitting region via a comparison with the low-ionization lines. We use the $C\ IV$ line, the most prominent metal line, to represent high-ionization lines, while we adopt $Mg\ II$ as a representation of low-ionization lines. Both lines are observable in SDSS AGNs at redshift $z \sim 2$, from which a sufficiently large sample can be obtained for our purpose. Please see Section 2 for the sample selection. We present in Section 3 the correlations between the properties of $C\ IV$ line, and the composite spectra. In Section 4, we examine whether the $C\ IV$ and $Mg\ II$ line properties follow the same correlations. Similarity in the correlations indicates that two lines come from regions with similar kinematics, while opposite results mean that the structures are different. Our method differs from earlier investigations, in which the authors directly compared the properties of the two lines. Then, in Section 5, we analyze the geometry and kinematics of the $C\ IV$ region and discuss the candidate models. We also present a comprehensive comparison between BAL and the blueshifted $C\ IV$ BEL. Finally, we summarize our results in Section 6.

2. Sample and Data Analysis

We select AGNs in the redshift range $1.7 < z < 2.2$ from the Fifth Data Release (DR5) of SDSS spectroscopic database (Schneider et al. 2007). The redshift range is chosen in such a way that both the $C\ IV$ and $Mg\ II$ lines fall in the wavelength coverage of the SDSS spectrograph. To ensure reliable measurements of emission line parameters, we only select objects with median signal-to-noise ratio $(S/N) \geq 7$ per pixel in both the $C\ IV$ (1450-1700 Å) and the $Mg\ II$ (2700-2900 Å) spectral regions. We further discard the broad absorption line

AGNs as cataloged by Scaringi et al. (2009). 6009 AGNs meet these criteria. The SDSS spectra are corrected for the Galactic extinction using the extinction map of Schlegel et al. (1998) and the reddening curve of Fitzpatrick (1999), and transformed to the rest frame using the improved redshifts for SDSS AGNs as computed by Hewett & Wild (2010, hereafter HW10). To measure the broad lines, we perform continuum and emission-line fitting using Interactive Data Language (IDL) code based on MPFIT (Markwardt 2009), which performs χ^2 -minimization by the Levenberg-Marquardt technique.

The Mg II broad lines are fitted using the exactly same method as Wang et al. (2009a). Here we only present a brief description of the procedures. First, we simultaneously fit the featureless continuum (assumed to be a power law) and the Fe II multiplet emission, which together constitute the so-called pseudocontinuum. Fe II is modelled with the tabulated semi-empirical template generated by Tsuzuki et al. (2006) based on their measurements of I ZW1; in the wavelength region covered by the Mg II emission, this template uses the calculation with the CLOUDY photoionization code (Ferland et al. 1998). After subtracting the fitted pseudocontinuum, the broad components of the Mg II $\lambda\lambda 2796, 2803$ doublet lines are each modelled with a truncated five-parameter (p_i , $i=0$ to 4) Gauss-Hermite series profile (van der Marel & Franx 1993). The expression for a Gauss-Hermite function is

$$\begin{aligned} G_h(x) &= p_0 e^{-x^2/2} [1 + p_3 h_3(x) + p_4 h_4(x)], \\ h_3(x) &= \frac{1}{\sqrt{6}} (2\sqrt{2}x^3 - 3\sqrt{2}x), \\ h_4(x) &= \frac{1}{\sqrt{24}} (4x^4 - 12x^2 + 3). \end{aligned}$$

where $x = (\lambda - p_1)/p_2$. The narrow component of each line is fitted with a single Gaussian. The full width at half maximum (FWHM) is measured from the Gauss-Hermite model of Mg II $\lambda 2796$, and rest equivalent width (EW) is the sum of the broad doublet lines.

To measure the C IV broad lines, we first fit the local continuum with a power-law in two wavelength windows near 1450Å and 1700Å, that have little or no contamination from emission-lines. After subtracting the continuum, we fit the residual spectrum around C IV with two Gaussians. Since the red wing of C IV is contaminated by He II, only the spectral region of 1450-1580Å is considered in fitting the C IV line. We also attempted to fit the residual spectrum with three Gaussians, which results in little or no significant improvements. We thus adopt the two-Gaussian model here.

In this work we introduce a blueshift and asymmetry index (BAI) to measure the deviation of the C IV line from an unshifted and symmetric profile. BAI is defined as the flux ratio of the blue part to the total profile, where the blue part is the part of C IV line at wavelengths short of 1549.06Å, the laboratory rest-frame wavelength of C IV doublets. The line parameters, BAI, FWHM and EW, of C IV are measured from the composite profiles of

the two-Gaussian model (in the wavelength range of 1450-1700Å). The BAI estimation may be affected by the accuracy of the redshifts which we use to transform the observed spectra to the rest frame. To reduce possible uncertainty of BAI thus introduced, we adopt the redshifts provided by HW10¹, which were derived by cross correlation of observed spectra with a carefully-constructed template. In particular, they corrected for the dependence of emission-line shift on luminosity and redshift, which is relevant to our investigation. BAI measures the combined effects of the asymmetry and shift of a line profile, which are generally treated separately in the literature (e.g. Sulentic et al. 2000a). In the Appendix we consider line shift and asymmetry separately and conclude that using BAI is a robust choice for our purposes. We use blueshift and BAI alternately in this paper.

The fitting results for most of the objects are reasonable according to our subsequent visual inspection. However, a small fraction of objects display strong narrow absorption in the emission lines regions, especially CIV spectral region, and cannot be well fitted by our automated processing. To minimize outliers left by the procedures, we eliminate objects with unacceptable fitting, i.e. $\chi^2/\text{d.o.f} > 1.5$. This restriction leads to a final working sample of 4963 AGNs. We note that the last selection has little or no effect on the results obtained in this paper.

3. Blueshift of CIV Emission Line

We show the distribution of BAI for the entire sample in Fig. 1. This parameter distributes in a wide range, from about 0.4 to more than 0.9, with a median value of 0.63. According to our definition of BAI, a blueshifted line has a BAI parameter larger than 0.5. Obviously, most of the AGNs in our sample display blueshifted CIV emission lines with respect to their systemic redshifts, in agreement with previous findings (Gaskell 1982; Richards et al. 2002). Only 7.2% of the AGNs are redshifted outliers. This fraction is the same as that found in Richards et al. (2011), in spite of that we adopt a different method to denote the blueshift. Since the blueshifted CIV line has been suggested to be emitted from outflows (e.g. Gaskell 1982; Murray & Chiang 1997; Leighly 2004), the BAI distribution suggests that outflows are common in AGNs.

We then show the equivalent width of CIV as a function of BAI and FWHM(CIV) in the two upper panels of Fig. 2. The CIV emission line is weaker for AGNs with larger blueshifts

¹More recently, Richards et al. (2011) also used these redshifts to compute the CIV line shift. They found that the resultant line-shift is consistent with the shift with respect to the low-ionization line MgII, which is often used in the literature.

or line widths. Both two trends are consistent with previous results. Richards et al. (2011) found an anti-correlation between blueshift and equivalent width (see also Marziani et al. 1996; Leighly & Moore 2004), and Wills et al. (1993) reported an anti-correlation of FWHM with EW. The left panel of Fig. 3 shows FWHM(CIV) against BAI. Our result confirms the finding of Richards (2006) that the line width of CIV is, on average, slightly larger for AGNs with larger blueshifts. Inspecting the scatter plot in detail, one can find that the trend is complex and there appears to exist a ‘V’-shaped lower envelope. It implies a mixture of origins of the CIV emission. We will come back to this issue later.

Composite spectra can provide a wealth of diagnostic information. We show the composite spectra as a function of BAI in Fig. 4. Our composites are constructed through the arithmetic mean method. We first sort the AGN sample according to their BAI then subdivide it into four equally-sized subsamples (each subsample contains about 1241 AGNs). For each AGN, we use the redshift from HW10 to deredshift the spectrum. The spectrum is then normalized at 1450\AA , rebinned into the same wavelength grids. The composite spectra are created by combining these normalized spectra in each of these subsamples. Only four major emission line regions, Si IV, C IV, C III] and Mg II, are presented. The spectra are normalized in the local continuum regions: (1355,1450), (1450,1700), (1830,1975), (2695,2955) (in units of \AA) for Si IV, C IV, C III] and Mg II.

As expected, the CIV emission line in our composites shifts significantly towards shorter wavelength as BAI increases. The equivalent width of CIV decreases with increasing BAI, consistent with Fig. 2. The blueshift is also remarkable for He II and moderate for Si IV, but seems to be absent in lower-ionization lines, such as Mg II and Al III, in good agreement with Richards et al. (2002). We also create composites as a function of EW(CIV) and BAI, following Richards et al. (2011). The composites are very similar to that shown in Richards et al. This is not surprising since we use the same AGN redshifts provided by HW10. Our composites reveal a significant excess flux in the blue wing of CIV (around 1500\AA), the strength of which increases with BAI (Fig. 2). We then take the difference between the largest-BAI and smallest-BAI composite spectra and show the difference as a function of velocity with respect to CIV in Fig. 5 (thick line). The blue excess wing peaks at 8000km s^{-1} , ranging between $\sim 4000\text{km s}^{-1}$ and 11000km s^{-1} .

Two additional phenomena are worth noting. First, the mean width of Mg II tends to be narrower for AGNs with larger CIV blueshifts. We will address this issue in next section. Second, the equivalent width of Al III is dramatically boosted at large BAI, different from other lines. Richards et al. (2011) paid particular attention to the unusual property of the Al III line. They suggested that the strong Al III, together with the large Si III]/C III] ratio, is indicative of an X-ray weak spectrum for these AGNs. Although this explanation

is reasonable, it might simply be that AlIII is contaminated by other lines. One possible contamination comes from the UV FeIII complexes. The FeIII complexes are usually more prominent on the long-wavelength side of CIII] (Laor et al. 1997). However, we do not find the expected excess at the corresponding wavelength and thus rule out this probability. Another promising explanation is that this excess flux is the CIII] emission of the outflow. To demonstrate this, we show the difference spectra of the largest-BAI and smallest-BAI composites as a function of velocity with respect to CIII] in Fig. 5 (thin line). One can find the average velocity of the ‘excess of AlIII’ is about 8000 km s^{-1} . This velocity is very similar to that of the blue wing excess of CIV and thus supports our interpretation. Difference spectra are usually sensitive to the normalization. To investigate into this, we also try to use other local continuum regions. The velocity ranges of the excess flux for both CIV and CIII] change only slightly.

The blueshifted CIII] component suggests that the number density of the large-velocity part of the CIV BELR cannot be much larger than $3 \times 10^9 \text{ cm}^{-3}$, which is the critical density of the intercombination line CIII] (Osterbrock 1989). This value is consistent with that estimated by Wang et al. (2009b), but much lower than that estimated by Ferland et al. (1992), about 10^{11} cm^{-3} (see also Kuraszkiewicz et al. 2000). The discrepancy can be understood if there exist two kinds of CIV emitting region: a normal gravitationally bound BELR and an outflow, as we will discuss in this paper. In fact, studies of blueshifted absorption lines revealed quite low densities in outflows (see Crenshaw et al. 2003 for a review). Moreover, the column density of outflow can be constrained based on the absence of blueshifted component in low-ionization line. For example, Leighly (2004) performed photoionization calculation to model the outflow components of various UV lines in two narrow-line Seyfert 1 galaxies and derived a rather low column density: $\log N_{\text{H}} \simeq 21.4$ for outflow gas. Leighly (2004) did not consider the blueshifted CIII] component. If taking into account this component, one may get a slightly larger column density. The lower density and column density than the typical values of normal emitting gas may be due to the expansion of outflow.

4. Comparison of Kinematics of MgII and CIV

In this section, we examine whether the MgII and CIV line properties follow the same correlations. Since MgII is thought to be emitted from a gravitationally bound BELR, the comparison may offer insight into the kinematics and geometry of the CIV emitting region. Note that our method differs from earlier investigations, in which the authors directly compared the properties of the two lines.

4.1. Correlations for Mg II and Fundamental Driver of C IV Blueshift

We show the rest equivalent width of Mg II against BAI and FWHM(Mg II) in the lower panels of Fig. 2. Note that the BAI presented here is calculated using C IV line. One can see that EW(Mg II) declines with increasing BAI. The trend is similar to but slightly weaker than C IV. Of particular interest is the positive correlation between EW(Mg II) and FWHM(Mg II), which is in contrast to C IV (Fig. 2). We also found such a correlation in a low-redshift AGN sample (Dong et al. 2009). The opposite behaviors indicates that the properties of Mg II and C IV emitting regions are essentially different.

The scatter plot of FWHM(Mg II) versus C IV blueshift is shown in the right panel of Fig. 3. Here again, we find a different correlation from C IV. AGNs with narrow Mg II BEL have a strong tendency to exhibit C IV emission with prominent blueshift. This trend is appreciable in previous work based on small low-redshift samples. For instance, Bachev et al. (2004) found the C IV blueshift can only be found in objects with FWHM(H β) less than 4000 km s⁻¹. Baskin & Laor (2005) found an marginal correlation between C IV blueshift and FWHM(H β) in 81 PG QSOs. Sulentic et al. (2007) used the centroid at half maximum of C IV profile as a surrogate of line shift. Their Figure 2 clearly shows a somewhat weak correlation between the blueshift and FWHM(H β) (see also Sulentic et al. 2000b). Since FWHM(Mg II) is closely correlated with FWHM(H β) (e.g. Wang et al. 2009a), their results broadly agree with ours.

This correlation hints that the C IV blueshift is driven by some primary physical parameters, such as black hole mass and the Eddington ratio² ($L_{\text{bol}}/L_{\text{Edd}}$). We calculate black hole masses based on the FWHM(Mg II) and the monochromatic luminosity $L_{3000} = \lambda L(3000\text{\AA})$ using the formula of Wang et al. (2009a)³. We then compute the Eddington ratio assuming a constant bolometric correction, $L_{\text{bol}} \simeq 5.9 L_{3000}$ (McLure & Dunlop 2004). To give a quantitative analysis, we perform Spearman rank correlation tests over the correlations of BAI with $L_{\text{bol}}/L_{\text{Edd}}$, M_{BH} and FWHM(Mg II), but note that these properties are degenerate, with $L_{\text{bol}}/L_{\text{Edd}} \propto \text{FWHM}^{-2}$, and $M_{\text{BH}} \propto \text{FWHM}^2$. The correlations with $L_{\text{bol}}/L_{\text{Edd}}$ and FWHM(Mg II) are comparable in strength, with Spearman correlation coefficients r_s of 0.54 and -0.50 respectively (the probabilities for null hypothesis are less than 10^{-100}), and are both significantly stronger than the dependence on M_{BH} ($r_s = -0.39$). Eddington ratio is therefore a more fundamental driver of the C IV blueshift than black hole mass. In Fig. 6,

² L_{bol} is the bolometric luminosity and L_{Edd} is the luminosity required for radiation pressure arising from electron scattering to balance the gravity of the central black hole.

³Our tests show that the results presented below do not change if we adopt other Mg II black hole mass formulae.

we show BAI as a function of $L_{\text{bol}}/L_{\text{Edd}}$. As $L_{\text{bol}}/L_{\text{Edd}}$ increases from 0.1 to 1, the median value of BAI significantly increases from ~ 0.5 to ~ 0.75 . A commonly accepted view for this correlation is that outflow is driven by radiation pressure (e.g. Murray et al. 1995; Boroson 2002), and therefore prominent for high $L_{\text{bol}}/L_{\text{Edd}}$ AGNs. If outflow carries away a significant amount of the angular momentum (e.g. Wang et al. 2007), it can serve as a driver of the accretion process, and consequently strengthen this correlation.

The correlation of BAI with FWHM(Mg II) is as strong as that with the Eddington ratio. It would be interesting to know which physical property dominates the correlations involving BAI. However, given the tight correlation between FWHM(Mg II) and the Eddington ratio ($r_s = -0.93$) in our sample, that is flux limited, it is impossible to disentangle these dependencies. A sample of AGNs covering a wide range in luminosity is required for this purpose. Recently, Richards et al. (2011) reported that the reverberation mapped AGNs occupy only part of the C IV line parameter space, and suggested that these objects have different ionizing spectral energy distribution (SED) from the mean SED of AGNs. It is unclear whether applying the scaling relation to the whole sample would lead to systematic error in determining M_{BH} and $L_{\text{bol}}/L_{\text{Edd}}$. If yes, the origin of the correlation between BAI and the inferred $L_{\text{bol}}/L_{\text{Edd}}$ would be more complex than that we discussed above, because the ionizing SED also correlates with the C IV blueshift (Richards et al. 2011). Even so, it doesn't necessarily mean the relationship between real $L_{\text{bol}}/L_{\text{Edd}}$ and BAI is weaker than that shown in Fig. 6. In fact, the correlation between SED, characterized by the ratio of X-ray flux to UV flux (α_{ox}), and the inferred $L_{\text{bol}}/L_{\text{Edd}}$ and line width is weak or absent (Vasudevan & Fabian 2007; Shemmer et al. 2008). These results doesn't favor that the estimates of $L_{\text{bol}}/L_{\text{Edd}}$ and M_{BH} are significantly affected by the assumption of a single mean SED. However, α_{ox} cannot fully characterize the ionizing SED, further work is needed. Moreover, the constant bolometric correction may introduce systemic bias in the dependence of BAI on $L_{\text{bol}}/L_{\text{Edd}}$. But it is not important here because the bolometric corrections differ between objects by a factor of 2 (e.g. Richards et al. 2006), much less than the $L_{\text{bol}}/L_{\text{Edd}}$ range of our sample.

4.2. C IV in High and Low $L_{\text{bol}}/L_{\text{Edd}}$ AGNs

When considering the correlations involving FWHM, we can see very different or even opposite behaviors between C IV and Mg II. FWHM may be a key to understanding the difference between C IV and Mg II emitting regions. The width of an emission line reflects the motion of the corresponding emitting gas. Mg II gas is thought to be gravitationally bound, whereas C IV line is generally blueshifted and the corresponding emitting gas may be

impacted or driven by the radiation field. Thus, $\text{FWHM}(\text{Mg II})$ is a measure of the gravity, while $\text{FWHM}(\text{C IV})$ is more likely the result of the competition between gravity and radiation pressure. It is therefore not surprising to find inconsistent trends. In order to understand the detailed effect of radiation pressure on C IV gas, it is necessary to explore more differences between Mg II and C IV, and to examine whether these trends for C IV hold for AGNs of different Eddington ratio.

To do so, we select two extreme subsamples which comprise the 25% highest $L_{\text{bol}}/L_{\text{Edd}}$ and 25% lowest $L_{\text{bol}}/L_{\text{Edd}}$ AGNs, designated as sample A and B respectively. We first show the $\text{FWHM}(\text{C IV})$ as a function of BAI for these two subsamples in the left panels of Fig. 7. There is a clear trend that C IV line width increases with BAI in sample A, but this trend disappears in sample B. An evidence for this discrepancy can also be found in the entire sample (left panel of Fig. 3). For comparison, we also show $\text{FWHM}(\text{Mg II})$ versus BAI for the *entire* sample in the same two panels (black points) as background. The C IV line of AGNs in sample A reveals an opposite tendency compared to the low-ionization line Mg II, while the C IV distribution of sample B is well consistent with the upper half of the Mg II distribution. We then make the same analysis of the FWHM-EW correlations for both lines and obtain similar results (see the right panels of Fig. 7). On one hand, AGNs in sample A exhibit a strong anti-correlation between $\text{FWHM}(\text{C IV})$ and $\text{EW}(\text{C IV})$, which is completely opposite to the correlation for Mg II. This correlation also exists in the whole sample, albeit weaker. On the other hand, for sample B AGNs, the correlation becomes marginal and the discrepancy between C IV and Mg II become tiny compared to sample A.

We note that the results shown above do not change if we select subsamples based on $\text{FWHM}(\text{Mg II})$ rather than $L_{\text{bol}}/L_{\text{Edd}}$. That is again due to the fact that $\text{FWHM}(\text{Mg II})$ is strongly correlated with Eddington ratio in our flux limited sample. Using 130 low-redshift AGNs with HST ultraviolet-band spectroscopic observation, Sulentic et al.(2007) found $\text{FWHM}(\text{C IV})$ increases with the blueshift *only* in AGNs with $\text{FWHM}(\text{H}\beta) \leq 4000 \text{ km s}^{-1}$. Their results are consistent with ours based on a much larger sample and Mg II, supporting that the kinematics of H β and Mg II regions are similar. They found AGNs with $\text{FWHM}(\text{H}\beta)$ less and greater than 4000 km s^{-1} exhibit different Fe II and radio properties and further suggested that there is apparent dichotomy between these two populations(see also Sulentic et al. 2000a;2000b; Bachev et al. 2004; Zamfir, Sulentic & Marziani 2008). We also find similar differences between sample A and B AGNs in the parameter space defined by BAI, FWHM and EW (and the same differences between the small and large $\text{FWHM}(\text{Mg II})$ subsamples). *More importantly, we find that the C IV emission of sample A is totally different from the low-ionization line Mg II, while the C IV emission of sample B is similar to Mg II.* In addition, Fig. 3 and 6 show clearly that the C IV blueshift varies continuously and smoothly with $\text{FWHM}(\text{Mg II})$ and $L_{\text{bol}}/L_{\text{Edd}}$. This implies that the corresponding variation in the

properties of the C IV emitting region is smooth, rather than abrupt.

5. Discussion

In this section, we analyze the kinematics and geometry of the C IV region on the basis of the results presented above. Then we discuss candidate BELR models that can account for the specific behavior of C IV. To get more insight into the origin of the C IV blueshift, we finally present a comprehensive comparison between the C IV blueshift and BAL.

5.1. Gravitationally Bound and Radiation Driven Emission Line Regions

The C IV emission of the AGNs in sample A is strongly blueshifted, and it also displays an opposite tendency compared to Mg II in the parameter space defined by BAI, FWHM and EW. It is very likely dominated by outflow, whose velocity range can be roughly measured by FWHM(C IV). Further evidence for the outflow origin of the C IV blueshift is given by comparison of the blueshifted C IV and BAL (see Sect. 5.3), that is believed to be produced by outflows.

The correlation between FWHM(C IV) and BAI found from sample A can be easily understood in terms of outflows. In general, an outflow with a large terminal velocity tends to produce emission with a large blueshift and FWHM(C IV). However, not all outflow models can successfully reproduce such a relationship. One of the commonly proposed models is disk-like equatorial outflows with a small opening angle. In this model, outflows on the far and near sides emit redshifted and blueshifted C IV photons, respectively, at comparable amounts (see, e.g. Figure 7 of Murray & Chiang 1997). Only when viewed along the pole, the emission line is significantly blueshifted. Meanwhile, we will see a very narrow line because the line of sight is nearly perpendicular to the outflow velocity. It is inconsistent with our finding here. One solution is that, in the case of disk-like outflows, a large opening angle is required. Alternatively, the outflow is funnel like (see the geometry shown in Elvis 2000 and Wang et al. 2007), even close to the polar direction in some cases (e.g. Zhou et al. 2006; Wang et al. 2008). For a funnel-like outflow, the projected velocity of the far-side along the line of sight is so small that it contributes only little to the red side of the C IV emission⁴.

The strong anti-correlation between FWHM(C IV) and EW(C IV) in sample A suggests

⁴The emission from an counter outflow on the other side of a presumed optically thick accretion disk is blocked.

that the CIV emission is suppressed in outflows at high velocities. This can possibly be ascribed to that, with expansion, the density of high velocity outflow gets lower, in agreement with our finding that the blueshifted component of the CIII] emission is possibly enhanced in AGNs with large BAI (see section 3 and Fig. 4). However, as a major coolant of BELR, CIV may be insensitive to the change of the density. Alternatively, Murray & Chiang (1997) suggested that this correlation is related to the distribution of the launching radius of outflows. Detailed dynamical and photoionization model is needed to understand the underlying process.

Different from the case of sample A, the CIV emission of the AGNs in sample B nearly overlaps with MgII in the parameter space. In particular, the two lines have similar widths. To demonstrate this more clearly, we show the probability distribution of $\log(\text{FWHM}(\text{Mg II})/\text{FWHM}(\text{CIV}))$ in the left panel of Fig. 8, which peaks at zero, albeit a large scatter of 0.16 dex. For comparison, we also plot the result for sample A, show that CIV is much broader than MgII. The similarity between the widths of CIV and MgII suggests that they largely come from the same emitting gas, which should be optically thick to ionizing radiation. Considering that radiation pressure is not important for optically-thick clouds (e.g. Fabian et al. 2006; Marconi et al. 2008) and that MgII is a reasonable indicator of black hole mass, our results suggest that the kinematics of the CIV emission-line gas in these AGNs is primarily governed by gravity rather than by radiation field. This argument is also consistent with the facts that sample B AGNs have small blueshifts of CIV and weak radiation field compared to gravity for their low $L_{\text{bol}}/L_{\text{Edd}}$.

The most convincing evidence to date for the gravitationally dominated kinematics of the CIV regions, from reverberation mapping observations of local AGNs, includes similar response timescales of the blue and red wings of CIV, the correlation between the BELR size and line width (Gaskell 1988; Koratkar & Gaskell 1991; Korista et al. 1995; Peterson & Wandel 1999; 2000; Onken & Peterson 2002). We examine the Eddington ratio of these reverberation mapped objects listed in Koratkar & Gaskell (1991), Peterson & Wandel (2000), and Onken & Peterson (2002) by collecting data from the literature, and find that almost all of these have quite low Eddington ratio, generally less than 0.1 (see Wang et al. 2009a for black hole mass and luminosity data). Moreover, radio-loud AGNs have averagely lower Eddington ratios (e.g. Boroson 2002; Zamfir et al. 2008) and weaker CIV blueshifts in comparison with radio-quiet AGNs. Both results are in agreement with our conclusion that the CIV region tends to be gravitationally bound at low $L_{\text{bol}}/L_{\text{Edd}}$.

Therefore, our finding reconciles naturally previous contradictory results. The CIV region tends to be dominated by outflows in high Eddington ratio AGNs, and dominated by normal gravitationally bound BELR in low Eddington ratio AGNs. The emission strength

from these two regions varies with $L_{\text{bol}}/L_{\text{Edd}}$ in opposite directions, and BAI is a measure of their radio. For low-BAI AGNs, in which the outflow component is trivial, C IV is emitted primarily from the gravitationally bound region and is expected have a similar line width to Mg II. This is supported by the probability distribution of $\log(\text{FWHM}(\text{Mg II})/\text{FWHM}(\text{C IV}))$ for the 25% lowest-BAI AGNs, as shown in the right panel of Fig. 8. Interestingly, we find that the distributions of high- and low- $L_{\text{bol}}/L_{\text{Edd}}$ AGNs (sample A and B) on the FWHM-BAI plane join at $\text{BAI} \sim 0.6$ (Fig. 7). At this value the emission from the two regions may be comparable, and also the distributions of BAI for all the AGNs peak (Fig. 1). We thus conclude that the gravitationally bound and radiation driven C IV emitting regions coexist in most of the AGNs (see also Richards et al 2011), and there is no abrupt transition from one type to the other.

5.2. Models for Two C IV Regions

Extensive efforts have already been devoted to understanding how an outflow is launched from an accretion disk (e.g. Arav et al. 1994; Murray et al. 1995; Proga, Stone & Kallman 2000; Everett 2005). These studies showed that the radiation force arising from line absorption of the central UV continuum can accelerate outflows to velocities up to 10000-20000 km s^{-1} . In particular, Murray et al. (1995) derived an approximate mass loss rate carried by outflow (their equation 9), that is equivalent to the strength of outflow, and found that it increases with the Eddington ratio (see also Proga et al. 2000). This is consistent with our finding here in observation. Another important parameter that also has impact on outflows is the strength of the X-ray emission relative to the UV (denoted as α_{ox}). A hard ionizing continuum can over-ionize outflows so that the acceleration efficiency of line absorption is suppressed; whereas a soft ionizing continuum would allow the launch of a strong wind (see e.g. Murray et al. 1995). Recently, Richards et al. (2011) found that AGNs with larger C IV blueshifts are apparently weaker in X-ray relative to UV (see also Gibson et al. 2008), consistent with the theoretical expectation. Both the above facts strongly favor the line driven outflow model.

If α_{ox} decreases with increasing $L_{\text{bol}}/L_{\text{Edd}}$ the dependencies of the C IV blueshift on $L_{\text{bol}}/L_{\text{Edd}}$ and α_{ox} are possibly induced by the same underlying causal process. Recent studies have revealed a complicated relationship between the two parameters. Kelly et al. (2008) found that α_{ox} decreases with $L_{\text{UV}}/L_{\text{Edd}}$, but increases with $L_{\text{X}}/L_{\text{Edd}}$, where L_{UV} and L_{X} are the UV and X-ray luminosity, respectively. Such a difference might be ascribed to the bolometric corrections of these two bands, that change with $L_{\text{bol}}/L_{\text{Edd}}$ in different ways (Vasudevan & Fabian 2007). Vasudevan & Fabian (2007) directly calculated L_{bol} by

fitting the broad spectral energy distributions and didn’t find any relationship, while they pointed out that α_{ox} cannot characterize the full ionizing continuum. Shemmer et al. (2008) also found that the dependence of α_{ox} on $L_{\text{bol}}/L_{\text{Edd}}$ is rather weak. They suggested that this correlation is probably a secondary effect of the correlations of L_{UV} with $L_{\text{bol}}/L_{\text{Edd}}$ and α_{ox} . Thus the outflow strength might be affected by least two ‘independent’ quantities: the Eddington ratio and the relative strength of the ionizing continuum.

One prediction of the line-driven outflow model is that the correlation between the outflow strength and $L_{\text{bol}}/L_{\text{Edd}}$ depends on the ionizing continuum. In Fig. 6, we show BAI against $L_{\text{bol}}/L_{\text{Edd}}$ for the two subsamples that comprise the 25% largest EW(CIV) and 25% smallest EW(CIV) AGNs respectively. One can find that the correlation between BAI and $L_{\text{bol}}/L_{\text{Edd}}$ is apparently stronger in the small EW sample than in the large EW sample. Since EW(CIV) is strongly correlated with α_{ox} (e.g. Wang et al. 1998; Wu et al. 2009), it is reasonable to expect that the small-EW AGNs are relatively X-ray weak compared to the large-EW ones. The result shown here thus provides another piece of possible evidence to support the model.

A viable model for the CIV emitting region must also account for the weakening of the normal CIV BELs in high- $L_{\text{bol}}/L_{\text{Edd}}$ AGNs. One possible mechanism is the change of the ionization state of BEL clouds, as discussed in Leighly (2004). In that model, the ionizing continuum is filtered through an outflow before reaching the normal BELR. The outflow absorbs the photons that can produce highly ionized ions, such as C^{+3} and He^{+2} . As the outflow becomes stronger, the continuum filtering is more severe and high-ionization lines from the normal BELR become weaker. A shortcoming of this model is that it cannot explain the weakness of the low-ionization line MgII in large BAI (strong outflow) or high $L_{\text{bol}}/L_{\text{Edd}}$ AGNs (Fig. 2). Because the ionization state of the outflow is high, it can only absorb photons in the helium continuum, but is transparent to low-energy ionizing photons (Leighly 2004). Note that a high ionization state is required for the outflow as there is no significantly blueshifted component in low-ionization lines. Nevertheless, the ionization state-SED scenario cannot be ruled out. The low-energy ionizing continuum may be just intrinsically weak when a strong outflow is launched.

Another possible mechanism is that the amount of BEL clouds varies with $L_{\text{bol}}/L_{\text{Edd}}$. If radiation pressure can expel BEL clouds out of the BELR (Dong et al. 2009; 2011, see also Ferland et al. 2009), the suppression of the normal BEL in high- $L_{\text{bol}}/L_{\text{Edd}}$ AGNs can be easily explained. Since BEL clouds are usually dust free, the radiation pressure arises mainly from three processes: Thomson scattering, resonance scattering and ionization absorption. Thomson scattering is not favored since it is only important in AGNs with super Eddington luminosities. Resonance scattering is neither able to drive clouds, because

the internal velocity dispersion of a cloud is generally small and only tiny fraction of photons can be scattered. Recently, Fabian et al. (2006; see also Marconi et al. 2008) found that the radiation pressure arising from absorption of ionizing photons cannot be neglected. Assuming the fraction, f_a , of ionizing flux is absorbed by a cloud with column density N_H , we can derive the ratio of the radiation force (due to ionization absorption) to the gravitational force on the cloud:

$$R_f = \frac{F_r}{F_g} = \frac{\frac{L_{\text{ion}} f_a}{4\pi r^2 c}}{\frac{GM_{\text{BH}} N_H m_p}{r^2}} = \frac{b f_a}{\sigma_T N_H} \frac{L_{\text{bol}}}{L_{\text{Edd}}} \quad (1)$$

where G , c and σ_T are gravitational constant, light speed and Thomson cross section, L_{ion} the luminosity of ionizing continuum, $b = L_{\text{ion}}/L_{\text{bol}}$, and r the distance from the cloud to the central source. When $R_f > 1$, the radiation force overcomes the gravity of the central black hole, and the clouds can escape from the BELR. It sets a lower limit of the column density of clouds that can survive: $f_a N_t L_{\text{bol}}/L_{\text{Edd}}$, where $N_t = b/\sigma_T$.

There are two parameters, f_a and N_t , to be determined. f_a is dependent on ionization degree and column density. For the typical normal BELR, when $N_H > 1.2 \times 10^{21} \text{cm}^{-2}$, that is the column density at the hydrogen ionization front, the cloud is optically thick to the ionizing continuum and $f_a \approx 1$ (Ferland 1999; Marconi et al. 2008). For $N_H < 1.2 \times 10^{21} \text{cm}^{-2}$, ionization absorption becomes ineffective, i.e. $f_a \approx 0$. We then give a rough estimate of N_t assuming the ionizing continuum seen by the cloud is the same as what we observe. Approximating the continuum at wavelength short of 1200\AA as a power law with an index $\alpha_\nu = -1.57$ (Zheng et al. 1997; Telfer et al. 2000), L_{ion} is given by integrating over all ionizing frequencies (i.e. above the frequency of Lyman edge): $L_{\text{ion}} \simeq 1.5\lambda L_\lambda(1200\text{\AA})$. Then approximating the UV continuum between 1200\AA and 3000\AA as a power law with an index $\alpha_\lambda = -1.54$ (Vanden Berk et al. 2001), $\lambda L_\lambda(1200\text{\AA}) \simeq 1.64\lambda L_\lambda(3000\text{\AA})$. Adopting $L_{\text{bol}} \simeq 5.9\lambda L_\lambda(3000\text{\AA})$ (McLure & Dunlop 2004), we obtain $b \approx 0.41$ and $N_t \approx 6 \times 10^{23} \text{cm}^{-2}$.

As long as $L_{\text{bol}}/L_{\text{Edd}} \gtrsim 1.2 \times 10^{21}/6 \times 10^{23} = 2 \times 10^{-3}$, clouds with column density in the range between $1.2 \times 10^{21} \text{cm}^{-2}$ and $N_t L_{\text{bol}}/L_{\text{Edd}}$ can be blown away from the BELR. That is to say, the amount of BEL clouds that can survive near the central engine drops with increasing $L_{\text{bol}}/L_{\text{Edd}}$. Increasing $L_{\text{bol}}/L_{\text{Edd}}$ up to 0.1, the upper limit of the column density of expelled clouds increases to $6 \times 10^{22} \text{cm}^{-2}$; where clouds can effectively emit the low-ionization line Mg II. Note that the estimation of N_t is inexact, since it depends on whether the ionizing emission is isotropic, or is blocked by other BEL clouds (Gaskell 2009) and/or other structures (such as outflows, Leighly 2004). Nevertheless, the mechanism proposed here gives a promising explanation to the suppression of both the C IV and Mg II emission from the normal BELR in high- $L_{\text{bol}}/L_{\text{Edd}}$ AGNs.

5.3. Connection Between C IV Blueshift and BAL

One of the most prominent spectral features imprinted by outflows is the broad absorption line. We refer to outflows associated with BAL as BAL outflow, while that associated with blueshifted BEL as BEL outflow. The comparison below suggests that BAL and BEL outflows may represent the same physical component.

Richards et al. (2002) found that the emission line features, such as the C III] line complex⁵, He II and the red wing of C IV, are very similar between the composites of BAL AGNs and non-BAL AGNs with large C IV blueshift. The broad band SED also displays a similar trend. For a given UV luminosity, non-BAL AGNs with large blueshifts tend to be X-ray weak compared to those with small blueshifts (Richards et al. 2011). The X-ray emission of BAL AGNs is usually severely absorbed, and thus cannot be directly used for a comparison. After correction for absorption, Fan et al. (2009) found that the intrinsic X-ray emission of BAL AGNs is on average weaker than that of non-BAL AGNs of the same UV luminosity. In particular, they found that the intrinsic X-ray strength is anti-correlated with the absorption strength of the C IV BAL for BAL AGNs. It is consistent with the correlation for the C IV BEL.

More similarities can be found when looking at the correlations of the outflow properties with $L_{\text{bol}}/L_{\text{Edd}}$. In this work, we find that the BEL outflow is stronger at a higher $L_{\text{bol}}/L_{\text{Edd}}$ (Fig. 6). Similar correlations between the BAL properties and $L_{\text{bol}}/L_{\text{Edd}}$ have been reported previously. Boroson (2002) has shown that BAL AGNs tend to occupy the extreme end of the Boroson & Green (1992) Eigenvector 1, that is thought to be driven by the Eddington ratio. Recently, Ganguly et al. (2007) found the fraction of BAL AGNs, an indicator of the average covering factor of outflow, increases with the Eddington ratio (see also Zhang et al. 2010). They also found there appears to exist an overall upper-envelope of increasing v_{max} of BALs with increasing Eddington ratio. The correlations for the BAL outflows are consistent with but weaker than those for the BEL outflows. There may be a simple reason for this: BAL troughs hold only the information of outflow along the line of sight, and thus may be sensitive to the local structure; while BEL is an integral of emission over entire volume of the outflow and represents the overall properties.

The similarity between the BEL and BAL outflows can also be found directly from their own properties. The first is the maximal velocity, v_{max} . Gibson et al. (2009) have obtained the distribution of v_{max} for BAL AGNs, which ranges from $<5000\text{km s}^{-1}$ to $>20000\text{km s}^{-1}$, with a mean value of $\sim 12000\text{km s}^{-1}$. The maximal velocity of a BEL outflow for individual

⁵C III] line complex is composed of C III], Si III] and Al III.

AGN is hard to estimate. We estimate the average v_{max} of the BEL outflow from the difference spectra of the largest-BAI and smallest-BAI composites (Fig. 5). It is about 11000 km s^{-1} , similar to the BAL outflow. We then compare their ionization states. As discussed above, the absence of blueshifted Mg II suggests that the BEL outflows contain very few Mg^+ ions. The same condition also appears in the BAL outflows. About only 10% of the BAL AGNs exhibit Mg II BAL (e.g Trump et al. 2006; Zhang et al. 2010), suggesting the absence of Mg^+ ions in most of the BAL outflows.

Given the similarities shown above, the BAL outflows may also be responsible for producing the observed blueshifted BEL, at least for the strongest blueshifted BEL. When the line of sight to the continuum source intersects the outflow, BALs are produced in the AGN spectrum; otherwise, the AGN appears as a non-BAL AGN with blueshifted C IV. The frequency of occurrence of BAL in AGN spectra, the strength of BAL trough, and the blueshift of C IV are all enhanced as the outflow is boosted with increasing $L_{\text{bol}}/L_{\text{Edd}}$ and/or decreasing the intrinsic X-ray emission. A viable outflow model must simultaneously account for both, the absorption and emission of C IV. Future studies on AGN outflows can be proceed from these two different approaches. For example, it is possible to use reverberation mapping results of the blueshifted C IV line to estimate the distance of the BAL outflow to the central source, an important parameter for understanding the launch of the outflow (the difficulty lies in how one separates variation of the outflow component from that of the normal BEL). One may also use the X-ray emission of AGNs with strongly blueshifted C IV, rather than the entire sample, to characterize the intrinsic X-ray emission of BAL AGNs; the latter is generally strongly absorbed and hard to study directly. In addition, we note that resonance scattering of the continuum and emission lines by ions, such as C^{3+} and N^{4+} , in outflows may also contribute to the observed emission (e.g. Wang et al. 2010). That is to say, for proper modeling of the emission lines, especially C IV and N V with large blueshifts (a strong outflow and a weak normal BELR), the scattering emission must be taken into consideration.

6. Summary

There are two kinds of models proposed to describe the kinematics and structure of the BELR of high-ionization lines (e.g. C IV) in AGNs, namely, the outflow and gravitationally bound BELR, that are apparently mutually contradictory. In this paper we attempt to uncover the underlying physical process responsible for this difference, using 4963 AGNs in the redshift range $1.7 < z < 2.2$ selected from SDSS DR5.

We introduce a blueshift and asymmetry index (BAI) to measure the deviation of the C IV line from an unshifted and symmetric profile. BAI is defined as the flux ratio of the

blue part to the total profile, where the blue part is the part of the C IV line at wavelengths short of 1549.06\AA , the laboratory rest-frame wavelength of the C IV doublets. BAI actually measures the combined effect of asymmetry and shift of a line profile, which is generally treated separately in the literature. Since both asymmetry and line shift may be caused by the same physical process, BAI is the best choice for our purpose.

We confirm previous findings that the C IV BEL is generally blueshifted with respect to the systemic redshift, and there exist significant correlations among the BAI, the line width (FWHM) and the rest equivalent width (EW) of C IV. For comparison, we investigate the same relationships among the BAI of C IV, the FWHM and EW of the low-ionization line Mg II. Dramatic differences are found between these two lines. For the Mg II line, FWHM is positively correlated with EW, and inversely correlated with BAI. While for C IV, FWHM is anti-correlated with EW, and the correlation between FWHM and BAI is complex and significantly different from that for Mg II. Given that line profile reflects the kinematic properties of the emitting gas, our results demonstrate clearly that, in general, the C IV line comes from a region with the structure and kinematics fundamentally different from those of Mg II, which is thought to be gravitationally bound.

We find a prominent correlation between BAI and the Eddington ratio, that is consistent with theoretical expectation. This correlation, together with the previously known correlation between C IV blueshift and the X-ray to UV flux ratio, advocates strongly the view that outflows are driven by resonance line absorption. Interestingly, there exist a number of similarities between blueshifted emission lines and broad absorption lines in AGNs in, for instance, the maximal velocity, ionization state and the correlations with the Eddington ratio and with the X-ray to UV flux ratio. These suggest that the same outflow produces these two different phenomena observed.

We select two subsamples, one composed of the 25% highest and one of the 25% lowest Eddington ratio AGNs. In the high Eddington ratio subsample, $\text{FWHM}(\text{C IV})$ is positively correlated with BAI and anti-correlated with $\text{EW}(\text{C IV})$. Both correlations are opposite to those for Mg II and can be understood in terms of outflow. Whereas, for the low Eddington ratio subsample, these two correlations for C IV become marginal or absent. C IV overlaps almost completely with Mg II in the parameter space. In particular, the line width of C IV is, on average, the same as that of Mg II. We thus conclude that the C IV line in this subsample is emitted by optically-thick gas driven by gravity, similar to the Mg II line.

Our results further suggest that the two C IV emitting regions, gravitationally bound and radiation driven, coexist in most of the AGNs. The emission strengths of these two regions vary smoothly with $L_{\text{bol}}/L_{\text{Edd}}$ in opposite directions. The C IV emission is generally dominated by outflows at high Eddington ratios, while it is primarily emitted from the normal

gravitationally bound BELRs at low Eddington ratios. This explanation naturally reconciles the contradictory views proposed in previous studies. Viable models are also discussed that can account for both, the enhancement of outflow emission and the suppression of the normal BEL, in AGNs with high Eddington ratios.

We thank the referee, Gordon Richards, for his helpful suggestions that improved the paper. This work is supported by NSFC (11073017, 11033007, 10973013, 10973012, 11073019), 973 program (2007CB815405, 2009CB824800) and the Fundamental Research Funds for the Central Universities. Funding for the SDSS and SDSS-II has been provided by the Alfred P. Sloan Foundation, the Participating Institutions, the National Science Foundation, the U.S. Department of Energy, the National Aeronautics and Space Administration, the Japanese Monbukagakusho, the Max Planck Society, and the Higher Education Funding Council for England. The SDSS Web site is <http://www.sdss.org/>.

REFERENCES

- Arav, N., Li, Z.-Y., & Begelman, M. C. 1994, *ApJ*, 432, 62
- Baskin, A., & Laor, A. 2005, *MNRAS*, 356, 1029
- Bachev, R., Marziani, P., Sulentic, J. W., Zamanov, R., Calvani, M., & Dultzin-Hacyan, D. 2004, *ApJ*, 617, 171
- Bentz, M. C., Peterson, B. M., Pogge, R. W., Vestergaard, M., & Onken, C. A. 2006, *ApJ*, 644, 133
- Boroson, T. A., & Green, R. F. 1992, *ApJS*, 80, 109
- Boroson, T. A. 2002, *ApJ*, 565, 78
- Chiang, J., & Murray, N. 1996, *ApJ*, 466, 704
- Collin, S., Kawaguchi, T., Peterson, B. M., & Vestergaard, M. 2006, *A&A*, 456, 75
- Crenshaw, D. M., Kraemer, S. B., & George, I. M. 2003, *ARA&A*, 41, 117
- Davidson, K., & Netzer, H. 1979, *Reviews of Modern Physics*, 51, 715
- Done, C., & Krolik, J. H. 1996, *ApJ*, 463, 144

- Dong, X.-B., Wang, T.-G., Wang, J.-G., Fan, X., Wang, H., Zhou, H., & Yuan, W. 2009, *ApJ*, 703, L1
- Dong, X.-B., Wang, J.-G., Ho, L. C., Wang, T., Fan, X., Wang, H., Zhou, H., & Yuan, W. 2011, *ApJ* accepted (arXiv:0903.5020)
- Elvis, M. 2000, *ApJ*, 545, 63
- Everett, J. E. 2005, *ApJ*, 631, 689
- Fabian, A. C., Celotti, A., & Erlund, M. C. 2006, *MNRAS*, 373, L16
- Fan, L. L., Wang, H. Y., Wang, T., Wang, J., Dong, X., Zhang, K., & Cheng, F. 2009, *ApJ*, 690, 1006
- Ferland, G. J., Peterson, B. M., Horne, K., Welsh, W. F., & Nahar, S. N. 1992, *ApJ*, 387, 95
- Ferland, G. J., Korista, K. T., Verner, D. A., Ferguson, J. W., Kingdon, J. B., & Verner, E. M. 1998, *PASP*, 110, 761
- Ferland, G. J., Hu, C., Wang, J.-M., Baldwin, J. A., Porter, R. L., van Hoof, P. A. M., & Williams, R. J. R. 2009, *ApJ*, 707, L82
- Fitzpatrick, E. L. 1999, *PASP*, 111, 63
- Ganguly, R., Brotherton, M. S., Cales, S., Scoggins, B., Shang, Z., & Vestergaard, M. 2007, *ApJ*, 665, 990
- Gaskell, C. M. 1982, *ApJ*, 263, 79
- Gaskell, C. M. 1988, *ApJ*, 325, 114
- Gaskell, C. M., & Goosmann, R. W. 2008, arXiv:0805.4258
- Gaskell, C. M. 2009, *New Astronomy Review*, 53, 140
- Gibson, R. R., Brandt, W. N., & Schneider, D. P. 2008, *ApJ*, 685, 773
- Gibson, R. R., et al. 2009, *ApJ*, 692, 758
- Hewett, P. C., & Wild, V. 2010, *MNRAS*, 405, 2302
- Kaspi, S., Smith, P. S., Netzer, H., Maoz, D., Jannuzi, B. T., & Givon, U. 2000, *ApJ*, 533, 631

- Kaspi, S., Maoz, D., Netzer, H., Peterson, B. M., Vestergaard, M., & Jannuzi, B. T. 2005, *ApJ*, 629, 61
- Kelly, B. C., Bechtold, J., Trump, J. R., Vestergaard, M., & Siemiginowska, A. 2008, *ApJS*, 176, 355
- Koratkar, A. P., & Gaskell, C. M. 1991, *ApJS*, 75, 719
- Korista, K. T., et al. 1995, *ApJS*, 97, 285
- Krolik, J. H., Horne, K., Kallman, T. R., Malkan, M. A., Edelson, R. A., & Kriss, G. A. 1991, *ApJ*, 371, 541
- Krolik, J. H. 2001, *ApJ*, 551, 72
- Kuraszkiewicz, J. K., Wilkes, B. J., Czerny, B., Mathur, S., Brandt, W. N., & Vestergaard, M. 2000, *New Astronomy Review*, 44, 573
- Laor, A., Jannuzi, B. T., Green, R. F., & Boroson, T. A. 1997, *ApJ*, 489, 656
- Leighly, K. M. 2004, *ApJ*, 611, 125
- Leighly, K. M., & Moore, J. R. 2004, *ApJ*, 611, 107
- Lynden-Bell, D. 1969, *Nature*, 223, 690
- Marconi, A., Axon, D. J., Maiolino, R., Nagao, T., Pastorini, G., Pietrini, P., Robinson, A., & Torricelli, G. 2008, *ApJ*, 678, 693
- Markwardt, C. B. 2009, *Astronomical Society of the Pacific Conference Series*, 411, 251
- Marziani, P., Sulentic, J. W., Dultzin-Hacyan, D., Calvani, M., & Moles, M. 1996, *ApJS*, 104, 37
- McLure, R. J., & Jarvis, M. J. 2002, *MNRAS*, 337, 109
- McLure, R. J., & Dunlop, J. S. 2004, *MNRAS*, 352, 1390
- Murray, N., Chiang, J., Grossman, S. A., & Voit, G. M. 1995, *ApJ*, 451, 498
- Murray, N., & Chiang, J. 1997, *ApJ*, 474, 91
- Nagao, T., Marconi, A., & Maiolino, R. 2006, *A&A*, 447, 157
- O’Brien, P. T., et al. 1998, *ApJ*, 509, 163

- Onken, C. A., & Peterson, B. M. 2002, *ApJ*, 572, 746
- Onken, C. A., Ferrarese, L., Merritt, D., Peterson, B. M., Pogge, R. W., Vestergaard, M., & Wandel, A. 2004, *ApJ*, 615, 645
- Onken, C. A., & Kollmeier, J. A. 2008, *ApJ*, 689, L13
- Osterbrock, D. E. 1989, Research supported by the University of California, John Simon Guggenheim Memorial Foundation, University of Minnesota, et al. Mill Valley, CA, University Science Books, 1989, 422 p.,
- Peterson, B. M., & Wandel, A. 1999, *ApJ*, 521, L95
- Peterson, B. M., & Wandel, A. 2000, *ApJ*, 540, L13
- Proga, D., Stone, J. M., & Kallman, T. R. 2000, *ApJ*, 543, 686
- Rees, M. J. 1984, *ARA&A*, 22, 471
- Richards, G. T., Vanden Berk, D. E., Reichard, T. A., Hall, P. B., Schneider, D. P., SubbaRao, M., Thakar, A. R., & York, D. G. 2002, *AJ*, 124, 1
- Richards, G. T. 2006, *arXiv:astro-ph/0603827*
- Richards, G. T., et al. 2006, *ApJS*, 166, 470
- Richards, G. T., et al. 2011, *AJ*, 141, 167
- Scaringi, S., Cottis, C. E., Knigge, C., & Goad, M. R. 2009, *MNRAS*, 399, 2231
- Schlegel, D. J., Finkbeiner, D. P., & Davis, M. 1998, *ApJ*, 500, 525
- Schneider, D. P., et al. 2007, *AJ*, 134, 102
- Shemmer, O., Brandt, W. N., Netzer, H., Maiolino, R., & Kaspi, S. 2008, *ApJ*, 682, 81
- Sulentic, J. W., Marziani, P., & Dultzin-Hacyan, D. 2000a, *ARA&A*, 38, 521
- Sulentic, J. W., Zwitter, T., Marziani, P., & Dultzin-Hacyan, D. 2000b, *ApJ*, 536, L5
- Sulentic, J. W., Bachev, R., Marziani, P., Negrete, C. A., & Dultzin, D. 2007, *ApJ*, 666, 757
- Telfer, R. C., Zheng, W., Kriss, G. A., & Davidsen, A. F. 2002, *ApJ*, 565, 773
- Trump, J. R., et al. 2006, *ApJS*, 165, 1

- Tsuzuki, Y., Kawara, K., Yoshii, Y., Oyabu, S., Tanabé, T., & Matsuoka, Y. 2006, *ApJ*, 650, 57
- van der Marel, R. P., & Franx, M. 1993, *ApJ*, 407, 525
- Vanden Berk, D. E., et al. 2001, *AJ*, 122, 549
- Vasudevan, R. V., & Fabian, A. C. 2007, *MNRAS*, 381, 1235
- Vestergaard, M., & Peterson, B. M. 2006, *ApJ*, 641, 689
- Wang, T.-G., Lu, Y.-J., & Zhou, Y.-Y. 1998, *ApJ*, 493, 1
- Wang, H.-Y., Wang, T.-G., & Wang, J.-X. 2007, *ApJS*, 168, 195
- Wang, J., Jiang, P., Zhou, H., Wang, T., Dong, X., & Wang, H. 2008, *ApJ*, 676, L97
- Wang, J.-G., et al. 2009a, *ApJ*, 707, 1334
- Wang, T., Zhou, H., Yuan, W., Lu, H. L., Dong, X., & Shan, H. 2009b, *ApJ*, 702, 851
- Wang, H., Wang, T., Yuan, W., Wang, J., Dong, X., & Zhou, H. 2010, *ApJ*, 710, 78
- Weymann, R. J., Morris, S. L., Foltz, C. B., & Hewett, P. C. 1991, *ApJ*, 373, 23
- Wilkes, B. J. 1984, *MNRAS*, 207, 73
- Wills, B. J., Brotherton, M. S., Fang, D., Steidel, C. C., & Sargent, W. L. W. 1993, *ApJ*, 415, 563
- Wu, J., Vanden Berk, D. E., Brandt, W. N., Schneider, D. P., Gibson, R. R., & Wu, J. 2009, *ApJ*, 702, 767
- York, D. G., et al. 2000, *AJ*, 120, 1579
- Zamfir, S., Sulentic, J. W., & Marziani, P. 2008, *MNRAS*, 387, 856
- Zhang, S., Wang, T.-G., Wang, H., Zhou, H., Dong, X.-B., & Wang, J.-G. 2010, *ApJ*, 714, 367
- Zheng, W., Kriss, G. A., Telfer, R. C., Grimes, J. P., & Davidsen, A. F. 1997, *ApJ*, 475, 469
- Zhou, H., Wang, T., Wang, H., Wang, J., Yuan, W., & Lu, Y. 2006, *ApJ*, 639, 716

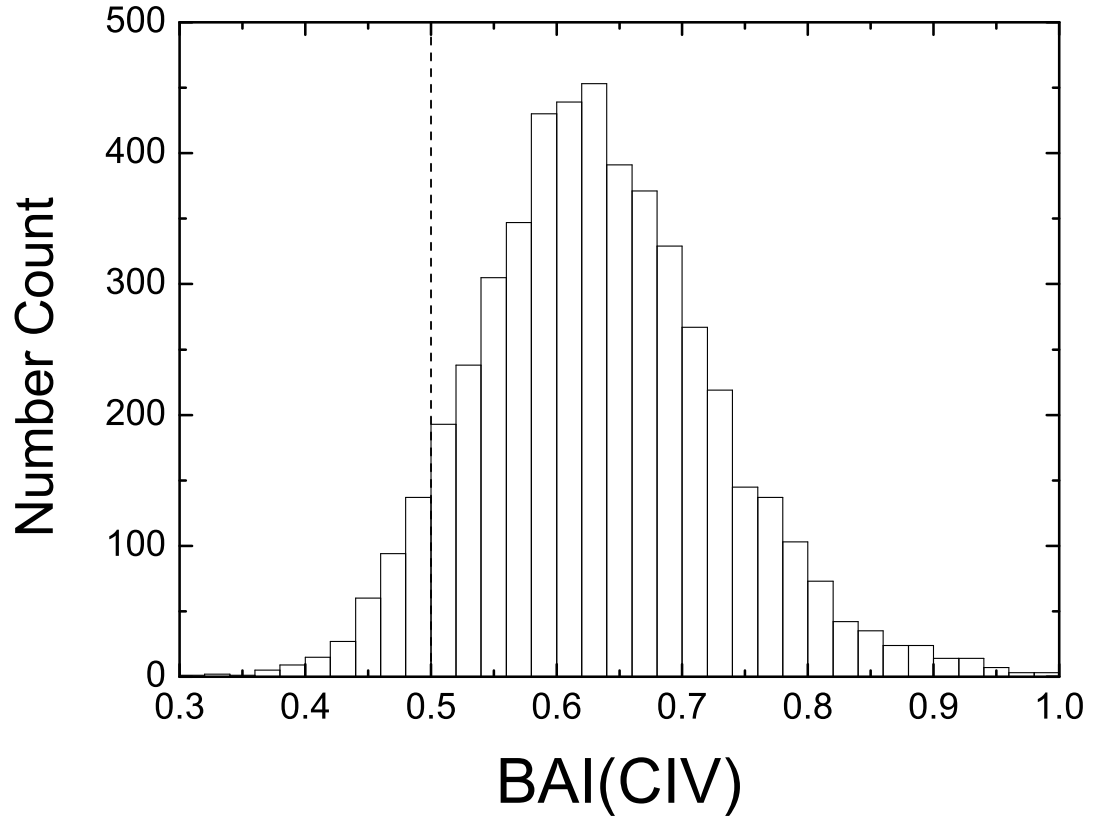


Fig. 1.— The distribution of blueshift and asymmetry index (BAI) for CIV BELs. The dashed line indicates an un-blueshifted CIV line profile.

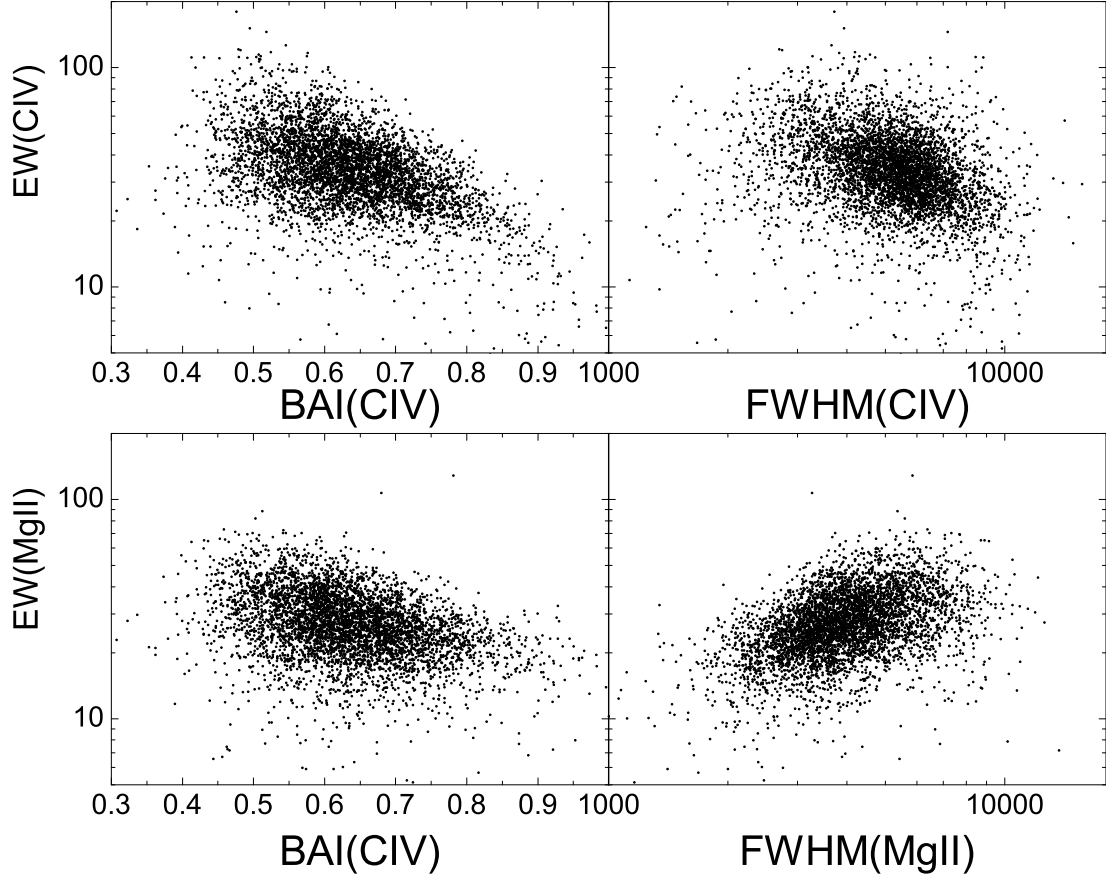


Fig. 2.— The rest equivalent width as a function of the full width at half maximum (FWHM) and BAI(CIV). The upper panels show the results for C IV, while the lower panels are for Mg II. Note that, in the lower left panel, BAI is calculated using the C IV BEL.

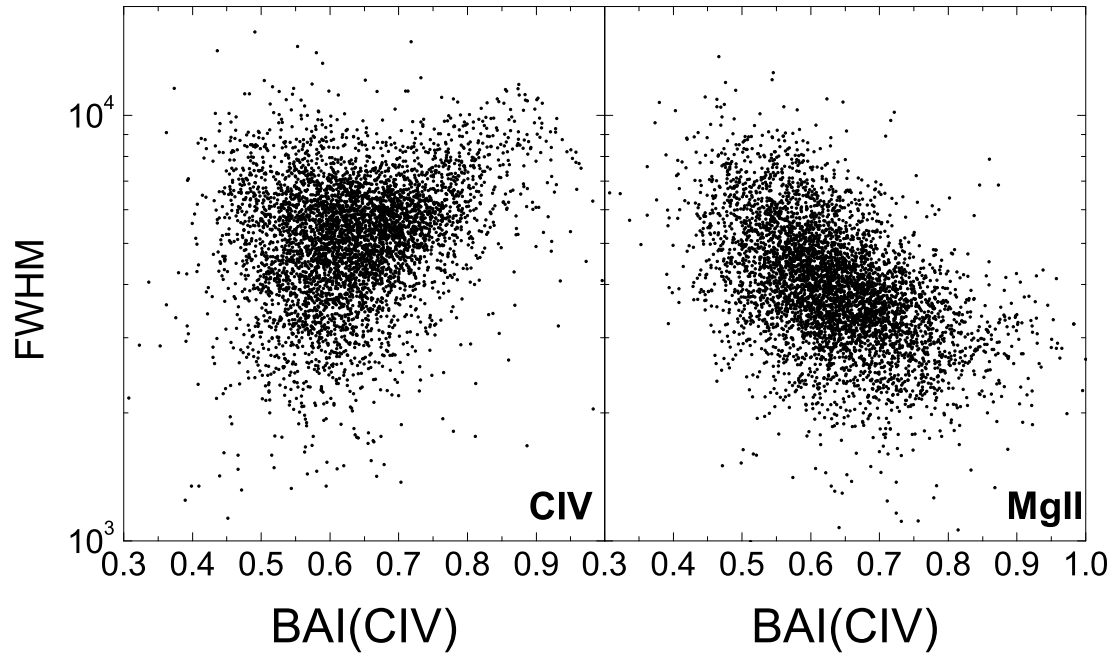


Fig. 3.— The left panel shows FWHM(CIV) versus BAI(CIV), while the right panel show FWHM(Mg II) versus BAI(CIV).

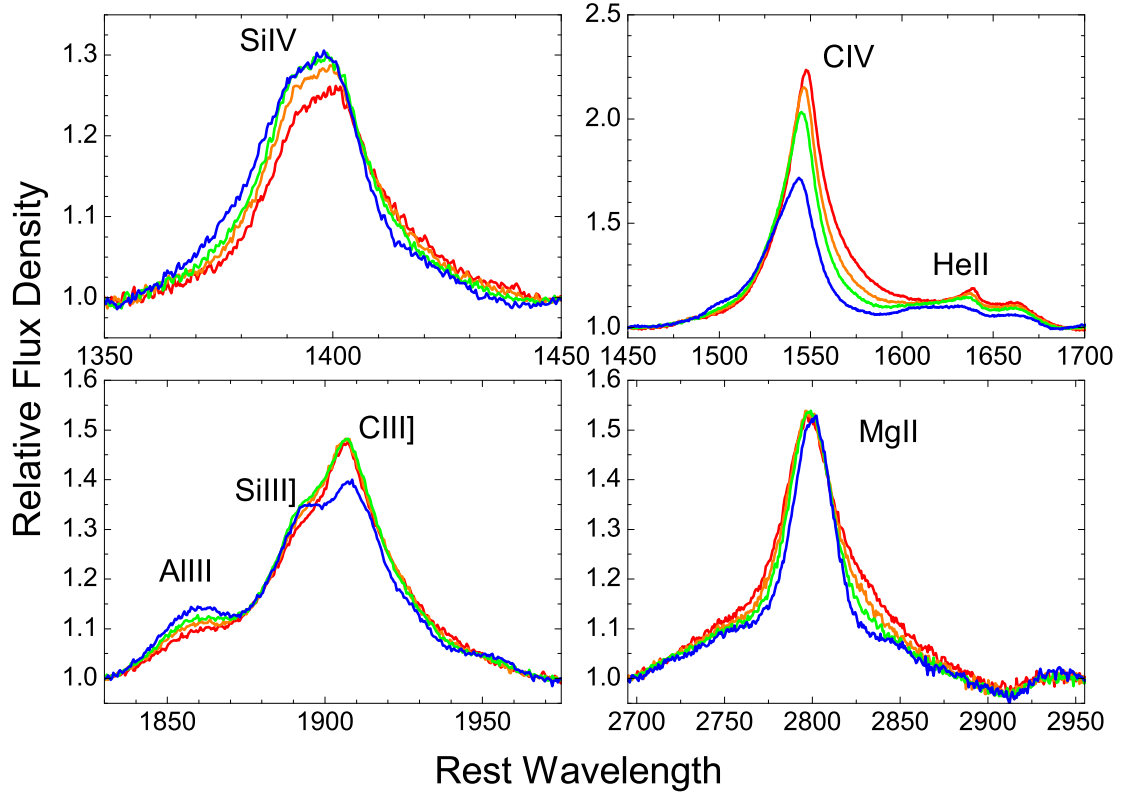


Fig. 4.— Strong emission lines region of the composite spectra. The spectra, in the order of increasing $\text{BAI}(\text{CIV})$, are plotted as red, orange, green and blue, respectively.

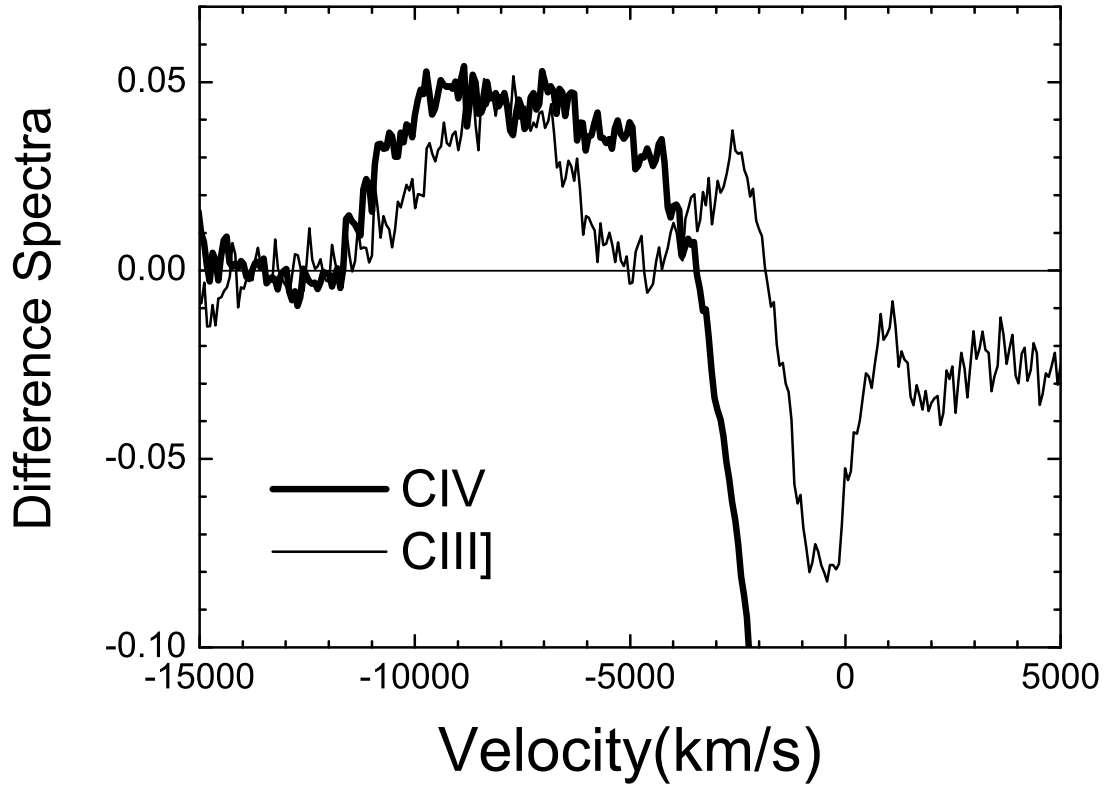


Fig. 5.— The difference between the largest-BAI(CIV) and smallest-BAI(CIV) composite spectra as a function of velocity with respect to both CIII](thin line) and CIV(thick line) respectively. Please see text for details.

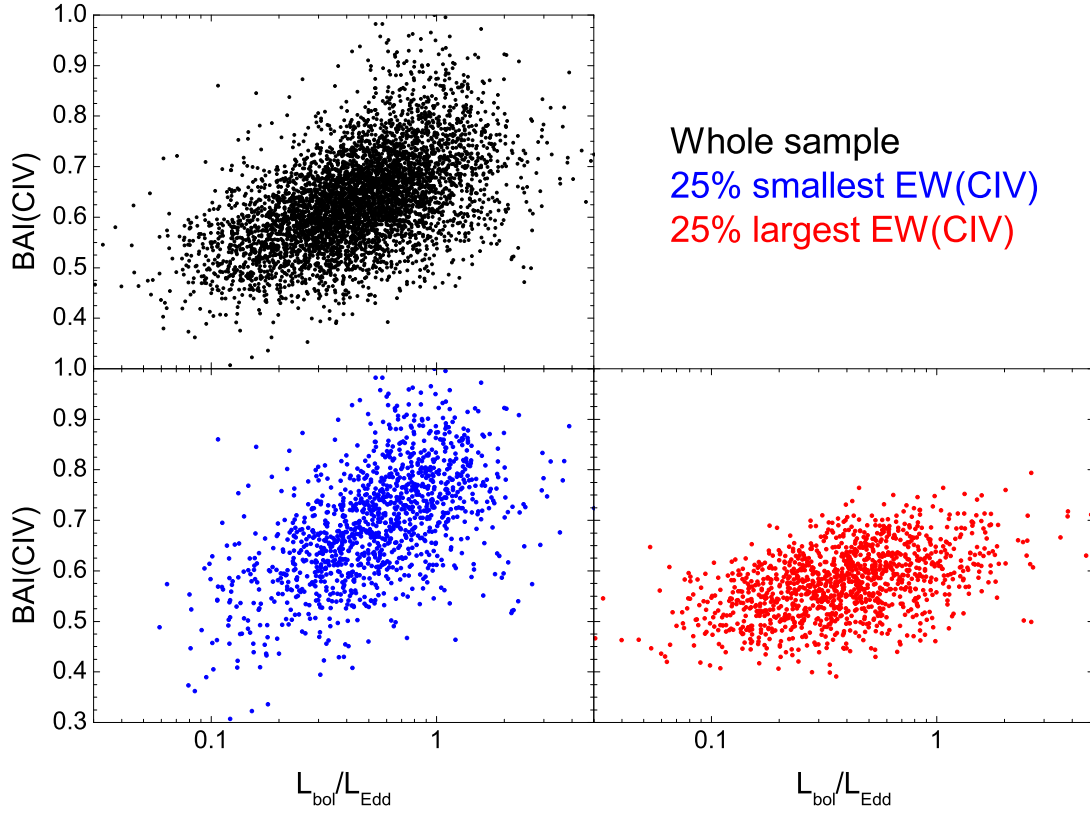


Fig. 6.— The CIV BAI as a function of the Eddington ratio, $L_{\text{bol}}/L_{\text{Edd}}$. The black hole mass and Eddington ratio is calculated based on Mg II mass formula in Wang et al. (2009a). The black points show the results for the whole sample. The red points are for 25% largest EW(CIV) AGNs, while the blue points are for 25% smallest EW(CIV) AGNs. For clarity, we don’t combine these panels.

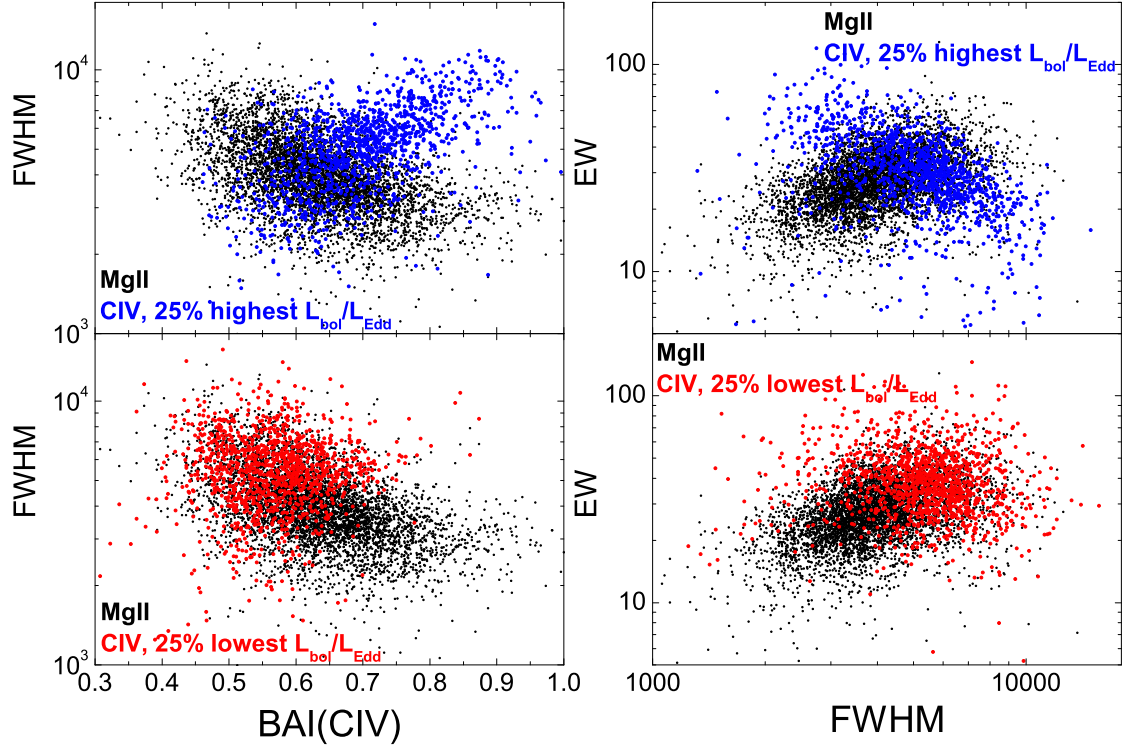


Fig. 7.— Left panels: FWHM versus BAI(CIV). Right panels: EW versus FWHM. The black points represent Mg II line, while the colored points are for CIV. The red points are for 25% lowest $L_{\text{bol}}/L_{\text{Edd}}$ AGNs (sample B), while the blue points are for 25% highest $L_{\text{bol}}/L_{\text{Edd}}$ AGNs (sample A). The black points are for the whole sample. For clarity, we don't combine these panels.

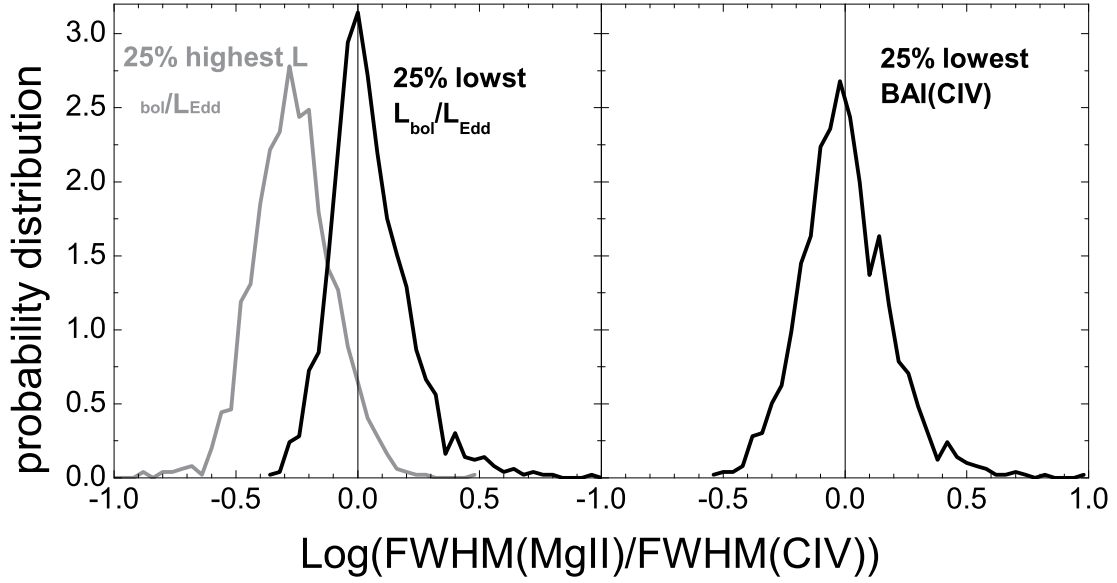


Fig. 8.— Left panel: the probability distributions of $\log \text{FWHM}(\text{Mg II})/\text{FWHM}(\text{C IV})$ for sample A (gray curve) and sample B (black curve). Right panel: the probability distribution for the 25% lowest $\text{BAI}(\text{C IV})$ subsample.

A. Notes on the asymmetry and shift of line profile

The asymmetry and shift of line profile are generally treated separately in the literature (e.g. Baskin & Laor 2005). Our blueshift and asymmetry index (BAI) is actually a combination of these two properties. In this Appendix, we present the line-shift index (SI) and asymmetry index (AI) of the CIV line profile and their comparisons with BAI. Both parameters are measured from the composite profiles of our two-Gaussian model. SI is defined as the shift of the line peak with respect to that in the AGN rest frame. Positive values of SI indicate blueshift. While AI is the flux ratio of the blue part to the total profile, where the blue part is the part of line profile at wavelengths short of the *peak wavelength*. The measurement of AI is therefore independent of the redshift errors of AGNs.

In the upper panels of Fig. 9, we show the distributions of AI and SI. The median of SI is about 898 km s^{-1} , in agreement with Richards et al. (2011). The median of AI is about 0.50, suggesting that there is no strong preference for red or blue asymmetries. This is consistent with the result in Marziani et al. (1996, their Figure 4, see also Sulentic et al. 2000a), but different from that in Baskin & Laor (2005), who found that the CIV lines tend to be blue asymmetric. To derive the line parameter, Baskin & Laor fitted the local continuum with a power-law in two wavelength windows near 1470 \AA and 1620 \AA . However, it is well known that there is a prominent bump near 1620 \AA (see e.g. Nagao et al. 2006). Adopting 1620 \AA as a continuum window can lead to systematic overestimation of AI.

AI and SI are strongly correlated with BAI (the lower panels of Fig. 9). The Spearman rank coefficients for these two correlations are both about $r_s = 0.7$, suggesting that redshift errors do not cause significant bias in BAI, at least for our sample with high S/N data. We use AI or SI, instead of BAI, to repeat our analysis. Interestingly, all the correlations shown in this paper retain, albeit becoming somewhat weaker. This means that we can draw the same conclusions by using any of these three parameters. This further suggests that the line asymmetry and line shift are caused by the same process, as is discussed in the main text. Since BAI is a combination of AI and SI, BAI is the best choice for our purpose here.

Moreover, we also attempt to use the often-used asymmetry index, such as the shift between the centroids at 1/4 and 3/4 maximum in units of FWHM (see Sulentic et al. 2000a; Baskin & Lasor 2005). Very similar results are obtained.

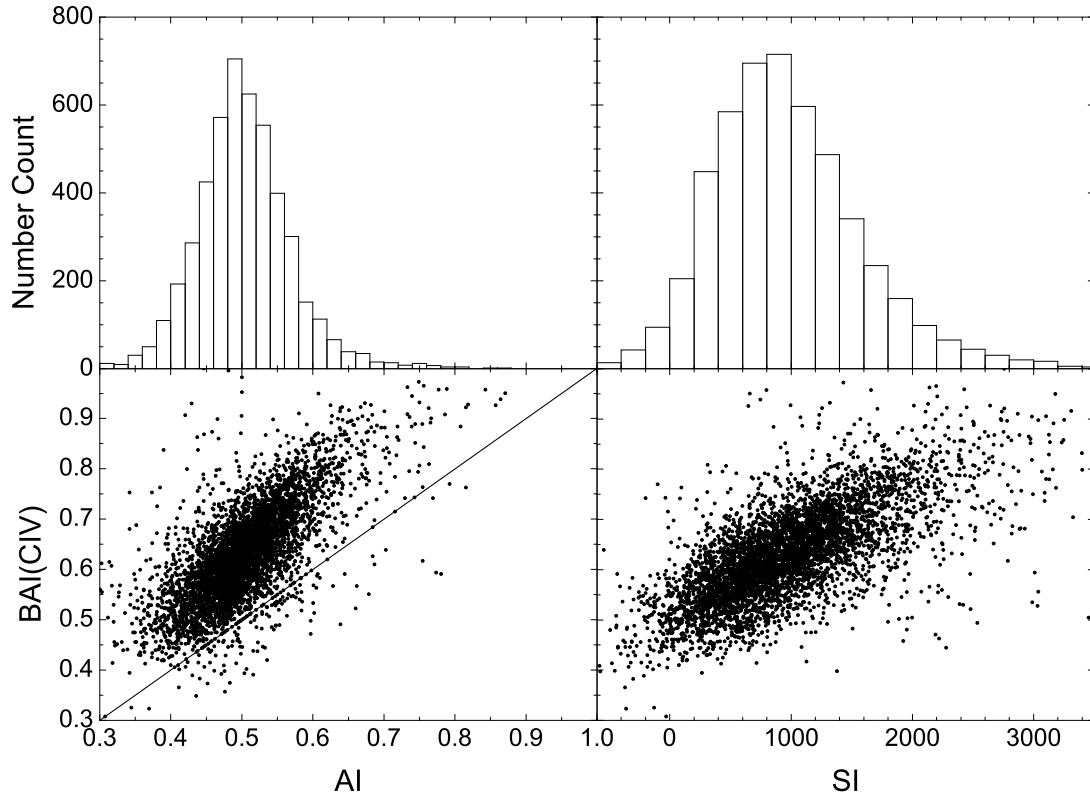


Fig. 9.— Upper-left panel: the distribution of asymmetry index (AI). Upper-right panel: the distribution of line-shift parameter (SI). Lower-left panel: BAI versus AI. Lower-right panel: BAI versus SI.